

Prediction of Polydisperse Steam Bubble Condensation in Sub-Cooled Water using the Inhomogeneous MUSIG Model

C. Lifante^{*}, T. Frank^{*}, A.D. Burns^{▲*}, D. Lucas[†] and E. Krepper[†]

^{*} ANSYS Germany GmbH, Staudenfeldweg 12, Otterfing, D-83624, Germany

[▲] School of Process Material and Environmental Engineering, CFD Centre, University of Leeds, LS2 9JT, UK

[†] Institute of Safety Research, Forschungszentrum Dresden-Rossendorf, POB 510 119, Dresden, D-01314, Germany

Email: Conxita.Lifante@ansys.com

Keywords: CFD, water/steam flow, MUSIG, polydisperse flow, phase change

Abstract

The aim of this paper is to present the validation of a new methodology implemented in ANSYS CFX (ANSYS, 2009), that extends the standard capabilities of the inhomogeneous MULTiple-Size Group model (MUSIG) by additionally accounting for bubble size changes due to heat and mass transfer. Bubble condensation plays an important role in sub-cooled boiling or steam injection into pools among many other applications of interest in the Nuclear Reactor Safety (NRS) area and other engineering areas. Since the mass transfer rate between phases is proportional to the interfacial area density, a polydisperse modelling approach considering different bubble sizes is of main importance, because an accurate prediction of the bubble diameter distribution is required.

The standard MUSIG approach is an inhomogeneous one with respect to bubble velocities, which combines the size classes into different so-called velocity groups to precisely capture the different behaviour of the bubbles depending on their size. In the framework of collaboration between ANSYS and the Forschungszentrum Dresden-Rossendorf (FZD) an extension of the MUSIG model was developed, which allows to take into account the effect of mass transfer due to evaporation and condensation on the bubble size distribution changes in addition to breakup and coalescence effects.

After the successful verification of the model, the next step was the validation of the new developed model against experimental data. For this purpose an experiment was chosen, which was investigated in detail at the TOPFLOW test facility at FZD. It consists of a steam bubble condensation case at 2MPa pressure in 3.9K sub-cooled water at a large diameter (DN200) vertical pipe. Sub-cooled water flows into the 195.3 mm wide and 8 m height pipe, where steam is injected at $z=0.0$ m and is recondensing. The experimental results are published in (Lucas, et al., 2007). Using a wire-mesh sensor technique the main characteristics of the two-phase flow were measured, i.e. radial steam volume fraction distribution and bubble diameter distribution at different heights and cross-sections.

ANSYS CFX 12.0 was used for the numerical prediction. A 60 degrees pipe sector was modelled in order to save computational time, discretized into a mesh containing about 260.000 elements refined towards the pipe wall and towards the location of the steam injection nozzles. Interfacial forces due to drag, lift, turbulent dispersion and wall lubrication force were considered. The numerical results were compared to the experimental data. The agreement is highly satisfactory, proving the capability of the new MUSIG model extension to accurately predict such complex two-phase flow.

Introduction

Computational Fluid Dynamics (CFD) simulations are increasingly used for analyses of potential accident scenarios in Nuclear Reactor Safety (NRS) analysis. Typical examples for the relevance of bubble condensation in NRS are sub-cooled boiling in core cooling channels or emergency cooling systems, steam injection into pools or steam bubble entrainment into sub-cooled liquids by impinging jets, e.g. in case of Emergency Core Cooling Injection (ECC) into a partially uncovered cold leg (Lucas et al., 2009). All these cases are connected with pronounced 3-dimensional flow characteristics, thus adequate simulations require the application of CFD codes.

Many activities were conducted in the last years to improve the modelling of adiabatic bubbly flows in the frame of CFD. In this case models for momentum transfer between the phases are most important. Usually they are expressed as bubble forces for interphase momentum transfer. Experimental investigations as well as Direct Numerical Simulations (DNS) showed that these bubble forces strongly depend on the bubble size. In addition to the well known drag force, also virtual mass, lift, turbulent dispersion and wall forces have to be considered (Lucas, et al., 2007). The lift force even changes its sign in dependence of the bubble size (Tomiyama, 1998) and Eötvös number. In consequence large bubbles are pushed to the opposite direction than small bubbles if a gradient of

the liquid velocity perpendicular to the relative bubble velocity exists (Lucas, et al., 2001) (Prasser, et al., 2007). To simulate the separation of small and large bubbles, more than one momentum equation is required (Krepper, et al., 2005) For this reason the so-called Inhomogeneous MUSIG (Multi Size Group) model was implemented into the ANSYS CFX code (Frank, et al., 2006) (Krepper, et al., 2005). It allows to consider a number of bubble sizes independently for the mass and momentum balance, also called *bubble classes*. For a proper modelling of bubble coalescence and breakup, a large number of bubble classes (e.g. 15-25) is required. Different independent groups of bubble classes can be considered for the momentum balance as well. They are called *velocity groups*. Fewer number of velocity groups (e.g. 2-3) are usually considered due to the high computational effort in solving individual sets of momentum transport equations. A common criterion for the classification can be derived from the dependency of the bubble forces on the bubble size, e.g. the change of the sign of the lift force. In the conventional version of the Inhomogeneous MUSIG model, only mass transfer between the bubble classes due to bubble coalescence and breakup can be modelled. In case of flows with phase change, additional transfers between the single classes and the liquid, and transfers between bubble classes caused by growth or shrinking of bubbles due to evaporation and condensation processes have to be considered. The additional terms for the extension of the MUSIG model are described later in the paper, and were implemented into a customized solver based on ANSYS CFX 12.

These extensions of the Inhomogeneous MUSIG model permit the simulation of flows with phase change. For a simulation based on physics, proper closure models for evaporation and condensation rates are further required. Usually these phase transfer rates are assumed to be proportional to the interfacial area density and the overheating or sub-cooling. For this reason detailed information on the evolution of local bubbles size distributions and local temperature profiles is needed. In the past, wire-mesh sensors were successfully used to measure local bubble size distributions in air-water (Lucas, et al., 2008) and adiabatic steam-water (Prasser, et al., 2007) flows in a vertical pipe. These data were used to validate models for bubble forces and to extent also models for bubble coalescence and breakup. Experiments using the wire-mesh sensor technology were done to investigate bubble condensation in an upwards directed vertical pipe. They clearly showed the effect of interfacial area density by comparison of experimental results for which only the initial bubble size distribution was modified by using different orifice sizes for bubble injection, but keeping the gas and liquid flow rates constant (Prasser, et al., 2007). The goal of this paper is to validate the extension of the Inhomogeneous MUSIG model against one of these condensation test case configurations.

Nomenclature

\vec{r}	Spatial position (m)
t	Time (s)
r_α	Phase volume fraction (-)
\vec{U}	Velocity (ms ⁻¹)
p	Pressure (Nm ⁻²)
\vec{S}_{MS_α}	Specified mass sources (N)
\vec{g}	Gravitational acceleration (ms ⁻²)
\vec{S}_{M_α}	Momentum sources (N)
\vec{M}_α	Interfacial forces (N)
\vec{F}_D	Drag force (N)
\vec{F}_L	Lift force (N)
\vec{F}_{WL}	Wall lubrication force (N)
\vec{F}_{VM}	Virtual mass force (N)
n	Bubble number density (kg ⁻¹ m ⁻³)
m	Mass (kg)
B_B	Bubble birth rate due to break up (kg ⁻¹ m ⁻³ s ⁻¹)
D_B	Bubble death rate due to break up (kg ⁻¹ m ⁻³ s ⁻¹)
B_C	Bubble birth rate due to coalescence (kg ⁻¹ m ⁻³ s ⁻¹)
D_C	Bubble death rate due to coalescence (kg ⁻¹ m ⁻³ s ⁻¹)
N_i	i-class bubble number density (m ⁻³)
f_i	i-class size fraction (-)
B_{B_i}	Discrete i-class bubble birth rate due to break up (kg ¹ m ⁻³ s ⁻¹)
D_{B_i}	Discrete i-class bubble death rate due to break up (kg ¹ m ⁻³ s ⁻¹)
B_{C_i}	Discrete i-class bubble birth rate due to coalescence (kg ¹ m ⁻³ s ⁻¹)
D_{C_i}	Discrete i-class bubble death rate due to coalescence (kg ¹ m ⁻³ s ⁻¹)
S_{fei}	Discrete mass transfer rate to class i due to phase change (kg ¹ m ⁻³ s ⁻¹)
g	Specific break up rate (kg ⁻¹ s ⁻¹)
Q	Specific coalescence rate (kg ¹ s ⁻¹)
X_{ijk}	Fraction of mass due to coalescence (-)
m_i	i-class bubble mass (kg)
J	Superficial velocity (ms ⁻¹)
T	Temperature (K)
ΔT	Sub cooling temperature (K)
D_i	i-class bubble diameter (Nm ⁻²)
a	Interfacial area density
A, B, \dots, R	Measurement elevations

Greek letters

Γ	Mass transfer rate (kgm ⁻³ s ⁻¹)
μ	Viscosity (Pas)
ρ	Density (kgm ⁻³)

Subscripts

S	Steam
W	Water
G	Gas
L	Liquid
S	Saturation
B	Break up
C	Coalescence
i	Bubble class
j	Velocity group
α, β	Phase name

inj Injection
ref Reference

Governing equations

The inhomogeneous Multiple Size Group model (MUSIG) is based on the Eulerian multiphase flow modeling approach (ANSYS, 2009)(Frank, et al., 2006). It is based on ensemble mass and momentum transport equations for all phases. Therefore, the continuity equations read as

$$\frac{\partial}{\partial t}(\mathbf{r}_\alpha \rho_\alpha) + \nabla \cdot (\mathbf{r}_\alpha \rho_\alpha \bar{\mathbf{U}}_\alpha) = \bar{\mathbf{S}}_{MS\alpha} + \sum_{\beta=1}^{N_p} \Gamma_{\alpha\beta} \quad (1)$$

where \mathbf{r}_α is the phase volume fraction, ρ_α the phase density, N_p the number of phases, $\bar{\mathbf{U}}_\alpha$ the phase velocity, $\bar{\mathbf{S}}_{MS\alpha}$ specified mass sources and $\Gamma_{\alpha\beta}$ is the mass flow rate per unit volume from phase β to phase α .

The phase- momentum equations read as:

$$\begin{aligned} & \frac{\partial}{\partial t}(\mathbf{r}_\alpha \rho_\alpha \bar{\mathbf{U}}_\alpha) + \nabla \cdot (\mathbf{r}_\alpha \rho_\alpha \bar{\mathbf{U}}_\alpha \otimes \bar{\mathbf{U}}_\alpha) = \\ & \nabla \cdot \left(\mathbf{r}_\alpha \boldsymbol{\mu}_\alpha \left(\nabla \bar{\mathbf{U}}_\alpha + (\nabla \bar{\mathbf{U}}_\alpha)^T \right) \right) - \mathbf{r}_\alpha \nabla p + \mathbf{r}_\alpha \rho_\alpha \bar{\mathbf{g}} + \\ & \sum_{\beta=1}^{N_p} (\Gamma_{\alpha\beta}^+ \bar{\mathbf{U}}_\beta - \Gamma_{\beta\alpha}^+ \bar{\mathbf{U}}_\alpha) + \bar{\mathbf{S}}_{M\alpha} + \bar{\mathbf{M}}_\alpha, \end{aligned} \quad (2)$$

where $\boldsymbol{\mu}_\alpha$ represents the phase viscosity, p the pressure, $\bar{\mathbf{g}}$ the gravitational acceleration, $\Gamma_{\alpha\beta}^+ \bar{\mathbf{U}}_\beta - \Gamma_{\beta\alpha}^+ \bar{\mathbf{U}}_\alpha$ describes the momentum transfer induced by mass transfer and $\bar{\mathbf{S}}_{M\alpha}$ refers to momentum sources due to external body forces and user defined momentum sources. $\bar{\mathbf{M}}_\alpha$ describes the interfacial forces acting on phase α due to the presence of other phases (drag, lift, wall lubrication, turbulent dispersion and virtual mass force):

$$\bar{\mathbf{M}}_\alpha = \bar{\mathbf{F}}_{\alpha,D} + \bar{\mathbf{F}}_{\alpha,L} + \bar{\mathbf{F}}_{\alpha,WL} + \bar{\mathbf{F}}_{\alpha,TD} + \bar{\mathbf{F}}_{\alpha,VM} \quad (3)$$

Since the sum of all phases must occupy the whole domain volume, the following constraint must be satisfied

$$\sum_{\alpha=1}^{N_p} \mathbf{r}_\alpha = 1 \quad (4)$$

Extension of the Inhomogeneous MUSIG model

The inhomogeneous Multiple Size Group model (MUSIG) assumes that the disperse phase is polydisperse, i.e. it is composed of different size particles (classes). This methodology can be applied both to bubbles and to droplets, although the work here presented is focussed on bubbly flows. The user selects a set of initial bubble diameters (d_i) and defines a reference density (ρ_{ref}), and the corresponding masses of the bubble classes are then

computed $\left(m_i = \frac{\pi}{6} \rho_{ref} d_i^3 \right)$. This is the value which is

going to characterize the class and remain constant during the simulation.

The different kinds of bubbles are then split into the so-called velocity groups, and all bubble classes in the same velocity group share the velocity field and other main variables. As mentioned, it is well-known that small and large bubbles behave in a significant different manner. Small bubbles flow with the fluid phase, large bubbles are more influenced by buoyancy. On the other hand side the lift coefficient changes its sign at a critical bubble diameter, which depends on the Eötvös number and hence on pressure and temperature. These are just some examples of the differences in the movement of bubbles of different size. In order to get an accurate prediction of the flow pattern, all these particularities must be solved. Defining different velocity groups for differently behaving groups of bubble size classes, these bubble size effects can be taken into account. Nevertheless, the standard formulation of the inhomogeneous MUSIG model allows only mass transfer between velocity groups due to break up and coalescence of bubbles. The extension of the method presented here considers mass transfer due to condensation or evaporation as well, i.e. the growth and shrink of the bubbles or even the appearance/disappearance of bubbles due to phase change are also considered. For this purpose the formulation of the MUSIG model has been modified, and one more term which accounts for the mass transfer due to phase change has been included.

The MUSIG model is a population balance approach, i.e. an equation for the bubble number density can be written. In its standard form the MUSIG model reads:

$$\begin{aligned} & \frac{\partial}{\partial t} n(\mathbf{m}, \bar{\mathbf{r}}, t) + \frac{\partial}{\partial \bar{\mathbf{r}}} (U(\mathbf{m}, \bar{\mathbf{r}}, t) n(\mathbf{m}, \bar{\mathbf{r}}, t)) + \\ & = B_B - D_B + B_C - D_C \end{aligned} \quad (5)$$

where n is the number of bubbles of mass m per cubic meter at position $\bar{\mathbf{r}}$ and time t . The four terms on the RHS of Eq. (5) correspond to the birth and death of bubbles due break up and coalescence, and can be written as:

$$B_B = \int_m^\infty g(\varepsilon; m) n(\varepsilon, t) d\varepsilon \quad (6)$$

$$D_B = n(\mathbf{m}, t) \int_0^m g(\varepsilon; m) d\varepsilon \quad (7)$$

$$B_C = \frac{1}{2} \int_0^m Q(\mathbf{m} - \varepsilon; \varepsilon) n(\mathbf{m} - \varepsilon, t) n(\mathbf{m}, t) d\varepsilon \quad (8)$$

$$D_C = n(\mathbf{m}, t) \int_0^\infty Q(\mathbf{m}; \varepsilon) n(\varepsilon, t) dt, \quad (9)$$

being $g(\mathbf{m}; \varepsilon)$ the specific breakup rate (the rate at which particles of mass m break into particles of mass ε and $m - \varepsilon$) and $Q(\mathbf{m}; \varepsilon)$ the specific coalescence rate (the rate at which particles of mass m coalesce with particles of mass ε to form particles of mass $m + \varepsilon$).

In order to extend the capabilities of the model in order to consider phase change effects, the following term was

included into the LHS of Eq. (5):

$$\frac{\partial n(m, \vec{r}, t)}{\partial m} \frac{\partial m(\vec{r}, t)}{\partial t} \quad (10)$$

The bubble number density equation (Eq. (5) + Eq. (10)) can now be discretized into size classes by integrating it between the limits of each bubble class. A bubble number density for each bubble class can then be defined as follows:

$$N_i(t) = \int_{m_i-1/2}^{m_i+1/2} n(m, t) dm \quad (11)$$

Since $m_i N_i = \rho_d f_i r_d$, being ρ_d the density of the disperse phase, r_d the volume fraction of the disperse phase, and f_i the size fraction of i -class bubbles, the extended equation can be re-written in terms of a size fraction equation as

$$\frac{\partial}{\partial t} (\rho_d r_d f_i) + \frac{\partial}{\partial X^j} (\rho_d r_d U_i^j f_i) = B_{B_i} - D_{B_i} + B_{C_i} - D_{C_i} + S_{fci} \quad (12)$$

being B_{B_i} , D_{B_i} , B_{C_i} , D_{C_i} the result of the mathematical manipulation of the corresponding break up and coalescence terms (B_B , D_B , B_C and D_C), and S_{fci} the transformation of the term in Eq. (10). The first four are:

$$B_{B_i} = \rho_d r_d \left(\sum_{j>i} g(m_j; m_i) f_j \right) \quad (13)$$

$$D_{B_i} = \rho_d r_d \left(f_i \sum_{j>1} g(m_i; m_j) \right) \quad (14)$$

$$B_{C_i} = (\rho_d r_d)^2 \left(\frac{1}{2} \sum_{j \leq i} \sum_{k \leq i} Q(m_j; m_k) X_{jki} f_j f_k \frac{m_j + m_k}{m_j m_k} \right) \quad (15)$$

$$D_{C_i} = (\rho_d r_d)^2 \left(\sum_j Q(m_i; m_j) f_i f_j \frac{1}{m_j} \right) \quad (16)$$

where

$$X_{jki} = \begin{cases} \frac{(m_j + m_k) - m_{i-1}}{m_i - m_{i-1}} & m_{i-1} < m_j + m_k < m_i \\ \frac{m_{i+1} - (m_j + m_k)}{m_{i+1} - m_i} & m_i < m_j + m_k < m_{i+1} \\ 0 & \text{otherwise} \end{cases} \quad (17)$$

is the fraction of mass due to coalescence between class j and k at time t which goes into class i . Finally the last term reads as:

$$S_{fci} = \begin{cases} \frac{m_i}{m_i - m_{i-1}} \Gamma_{i-1} - \frac{m_i}{m_{i+1} - m_i} \Gamma_i & \text{(evaporation)} \\ \frac{m_i}{m_i - m_{i-1}} \Gamma_i - \frac{m_i}{m_{i+1} - m_i} \Gamma_{i+1} & \text{(condensation)} \end{cases} \quad (18)$$

where m_i is the mass of bubbles in class i , and Γ_i the direct mass transfer per unit volume and time between the continuous liquid phase and the bubble size class i . These source terms reflect the effect of mass transfer between liquid and bubble size class i , as well as the transfer between MUSIG groups due to bubble growth or shrinking. This can be checked by considering the net transfer at the group boundary. In case of condensation, bubble sizes shrink, i.e. bubbles are shifted to smaller mass classes. Considering the net transfer at the lower boundary of bubble size group i there is a sink in bubble size group i

according to the Eq. (18) equal to $\frac{m_i}{m_i - m_{i-1}} \Gamma_i$. On the

other hand the related source in bubble size group $i-1$ is equal to $-\frac{m_{i-1}}{m_i - m_{i-1}} \Gamma_i$. Summation of gain and loss

results in $\frac{m_i - m_{i-1}}{m_i - m_{i-1}} \Gamma_i = \Gamma_i$.

Assuming spherical bubbles, the Sauter mean diameter for the velocity group j is obtained according to:

$$d_{s,j} = \frac{r_j}{\sum_i \frac{r_i}{d_i}} \quad (19)$$

The sum runs over all MUSIG classes i which belong to the velocity group j . The mass transfer for the MUSIG groups i is evaluated based on the Sauter mean diameter, the interfacial area density, and the mass transfer per unit volume and time for velocity group j (Γ_j):

$$\Gamma_i = \Gamma_j \frac{a_i}{a_j} = \Gamma_j \frac{6r_i/d_i}{6r_j/d_{s,j}} = \Gamma_j \frac{r_i}{r_j} \frac{d_{s,j}}{d_i} \quad (20)$$

where a represents the interfacial area density.

The mass transfer per unit volume and time for velocity group j (Γ_j) can be computed from the volume related heat flux to the interface and heat of evaporation

$$\Gamma_j = \frac{a_j}{H_{LG}} (h_{G,j}(T_G - T_s) - h_{L,j}(T_L - T_s)) \quad (21)$$

Herein T_G , T_L and T_s are the gas, liquid and saturation temperatures, H_{LG} the heat of evaporation, and $h_{G,j}$ and $h_{L,j}$ the heat transfer coefficients from gas and liquid side to the interface.

Validation case description

After the derivation of the model, and its implementation in a customized solver based on ANSYS CFX 12, a verification process was carried out. A collection of simplified test cases with given condensation or evaporation rates were analyzed and compared to their analytical solution. Several configurations regarding boundary conditions, bubble class and velocity group definitions were investigated, providing in all cases the same result as the analytical solution. Details of the verification are not included here and can be obtained from (Lifante, et al., 2009a) and (Lifante, et al., 2009b). Once the new implementation was completed, a complex validation case was chosen to test the adequateness of the model for applications where break up, coalescence and phase change take place simultaneously. The present work was performed in collaboration with the Forschungszentrum Dresden-Rossendorf, and a condensation case experimentally investigated at the TOPFLOW test facility was selected for the model validation.

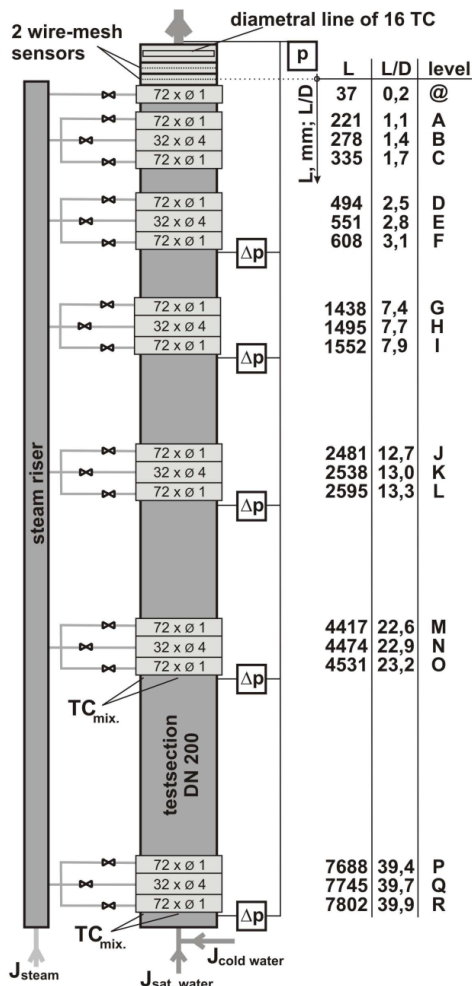


Figure 1: Geometry details of the TOPFLOW test facility at FZD (DN200 vertical pipe)

The TOPFLOW facility (see Figure 1) consists of a large vertical DN200 pipe (8 m height, 195mm pipe diameter). By means of injection chambers like the one in Figure 2 (left), gas can be injected into the fluid flowing through the

pipe at different height of the test section. In the investigated case sub cooled water was flowing upwards and steam was injected through 72 small injection nozzles of 1 mm diameter. Using a wire mesh sensor technique (Figure 2, right) (Prasser, et al., 2007) and placing it at a constant position at the end of the test section in varying distance to the used injection chamber, the experimentalists at FZD measured radial steam volume fraction distributions and radial bubble size distributions for different length of flow development in the pipe. These values were determined for the different elevations of the steam injection named with letters, being *A* the injection level closest to the sensors (22cm above it), and *R* the furthest (7.8 m below the wire-mesh sensors).

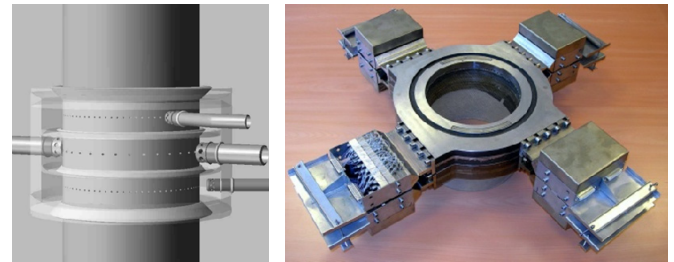


Figure 2: Left: Injection chamber at the TOPFLOW facility. Right: Wire mesh device.

Experimental results of the chosen configuration, in addition to many others, are compiled in (Prasser, et al., 2007). From the different arrangements investigated in that paper, the so-called run #3 is the one which is investigated in this paper by means of CFD simulation. The main physical properties defining this case are summarized in Table 1 :

Pres. [MPa]	J_w [m/s]	J_s [m/s]	T_w [°C]	T_s [°C]	ΔT_L [°C]	D_{inj} [mm]
2.0	1.0	0.54	214.4	210.5	3.9	1.0

Table 1: Main physical characteristics of the selected validation test case from TOPFLOW measurements.

Figure 3 shows the experimental results regarding the radial steam volume fraction distributions at the mentioned distances between steam injection and measurement cross-section. For level *A* a local maximum of about 30% can be observed, as expected from the ratio between the water and the steam superficial velocities in this particular test case. This large value evidences the complexity of the application. It can be noticed that substantial steam condensation is taking place along the pipe, and the larger is the injection-measurement distance, the lower amount of steam is present in the pipe.

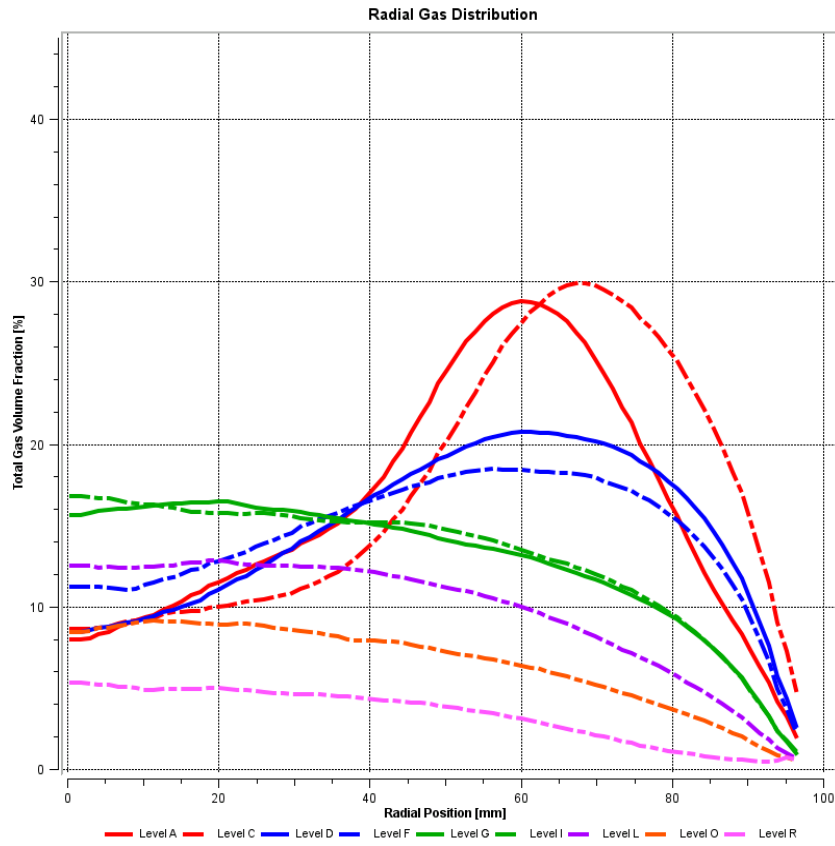


Figure 3: Experimental radial steam volume fraction distribution at different elevations (levels *A* to *R*)

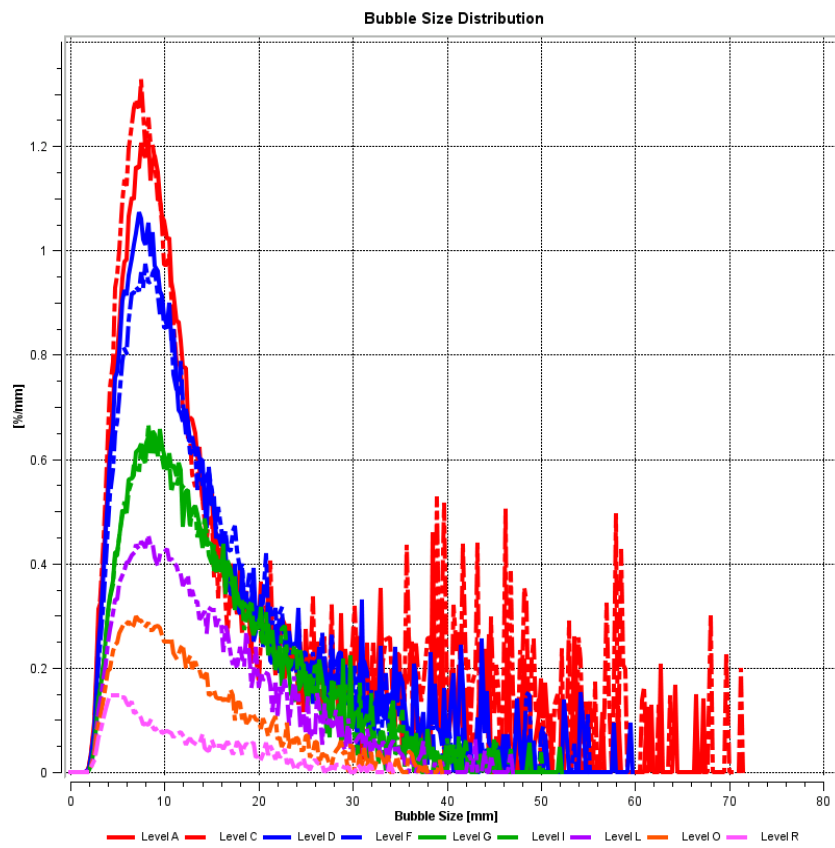


Figure 4: Radial bubble size distribution (dr_g/dD_B) at different elevations of steam injection (levels *A* to *R*)

In addition, Figure 4 shows the radial bubble size (diameter) distribution at the same elevations, represented by the quantity dr_g/dD_B . In this manner the cross-sectional average of the steam volume fraction can be computed by evaluating the integral area under each profile. The condensation effect is visible here as well since the enclosed area under the curves decreases along the pipe. Being this a condensation case, one would expect that the maximum of the mentioned curves (representing the most common bubble class at each elevation) is shifted towards smaller bubble diameters along the pipe. However, except for the upmost elevations, this value remains almost constant close to 9 mm. This indicates that not only condensation is playing a role in the application but coalescence as well. This was a further reason for choosing this case for the validation of the extension of the MUSIG model.

CFD Model validation – CFD Setup definition

A three-dimensional model containing one sixth of the geometry was considered for the numerical simulations. In this way the three-dimensional effects due to the steam injection through discrete nozzles can be reproduced, and computational time can be saved in comparison with the simulation of the whole domain. Symmetry boundary conditions were applied to the two side planes of the symmetry sector. An inlet boundary condition based on the water superficial velocity, outlet boundary condition based on averaged static pressure and adiabatic pipe wall were considered for the simulation. Since no experimental information about water velocity distribution or turbulence quantities at the pipe inlet was available, the computational domain was enlarged by two meters in front of the steam injection in order to ensure that the flow is completely developed when it reaches the steam injection locations.

A numerical grid containing 260.442 elements was employed. It was refined towards the wall and near the injection locations. No grid-independency analysis was performed because previous numerical studies for adiabatic air/water flow through the TOPFLOW test facility (Frank, 2006) carried out for several different superficial velocity ratios had proven the adequateness of this grid resolution.

The injection nozzles were modelled by means of source points located close to the wall. The original nozzle diameter in the experiments was 1 mm. Due to the large steam superficial velocity, this leads to an extreme large steam injection velocity

$$v_{inj} = \frac{1}{72} \frac{J_S R_{TOPFLOW}^2}{R_{inj}^2} = \frac{1}{72} 0.54 \frac{(0.195/2)^2}{(0.001/2)^2} = 285 \text{ m/s}$$

In initial investigations this had strongly deteriorated the convergence of the numerical simulations. Therefore, for part of the computations, a larger nozzle diameter was considered (4 mm), keeping the steam mass flow rate constant, but providing a lower injection velocity.

The turbulence of the continuous phase was modelled by the SST turbulence model (Menter, 1994). As in all multiphase applications, the consideration of the interfacial momentum, heat and mass transfer is crucial for the accuracy of the numerical results. In the present case Grace drag, Tomiyama lift and FAD turbulent dispersion force were considered, as well as the Tomiyama wall lubrication force (ANSYS, 2009).

Break up and coalescence were modelled following the standard approach in ANSYS CFX using the Luo & Svendsen and Prince & Blanch models respectively (Luo, et al., 1996) (Prince, et al., 1990). The corresponding break up factor (0.025) and coalescence factor (0.05) were chosen from previous investigations (Krepper, 2008).

The gaseous phase was assumed to be at saturation temperature and to be composed of 25 different bubble classes, distributed into three velocity groups, whose limits were

- First group → [0 mm, 3 mm]
- Second group → [3 mm, 6 mm]
- Third group → [6 mm, 30 mm]

The selection of the velocity group boundaries was chosen depending on the Eötvös number, which allows to predict the critical diameter at which the sign of the lift coefficient in the lift force formulation of Tomiyama changes. Using this value the different bubble classes were arranged into velocity groups where the coefficient is clearly positive, transitional or close to zero, or clearly negative.

Results and discussion

Figure 5 shows the radial steam volume fraction at level C (33 cm above the steam injection) for the different simulations conducted and the corresponding experimental values (crosses). Results corresponding to the first simulation (green dashed profile) show an over prediction of the local maximum amount of steam (55% against 30%), and additionally its location is shifted towards the wall in comparison with the experiments. This simulation allowed us to get detailed knowledge and to optimize the numerical parameters to reach convergence (like the necessary iteration time step among others). However, results were still far from the experiments. Therefore some changes/improvements in the setup were carried out. The first modification consisted of displacing the position of the source points (SP) from the wall to 75 mm away from the centre of the pipe. This was the location where the experimentalists at FZD observed the maximum concentration of steam at steam injection to measurement distance of level A. By applying this change, a reduction of the local maximum of steam and a displacement of it towards the centre of the pipe could be observed (brown dashed profile). Next step was the consideration of the wall lubrication force, which was not taken into account in the previous two simulations.

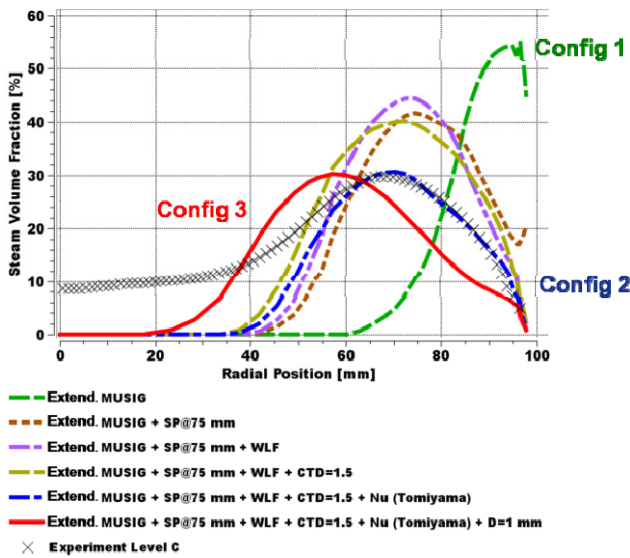


Figure 5: Radial steam volume fraction distribution at level C (33 cm above the injection level) for different setup configurations.

As expected the steam was thereby further kept away from the wall and for the steam volume fraction directly at the wall a more physical behavior could be observed. Further, the influence of the turbulent dispersion force was increased by enlarging the turbulent dispersion coefficient from 1.0 to 1.5 (dash dotted light green), which corresponds to the level of uncertainty regarding this model parameter in accordance to the model derivation by different authors in literature. A slight improvement could be observed. The parameter which had the largest influence in the numerical results was the correlation used for the heat transfer. First results were obtained using the Ranz-Marshall correlation. It was proven in this application, as well as in the literature, that this correlation under predicts the heat transfer and therefore the condensation rate in applications with large amount of steam and with bubble diameters larger than 1mm. Instead, a new correlation suggested by Prof. Tomiyama (Tomiyama, 2009) was implemented (blue profile), providing a satisfactory agreement with the experimental results regarding both the value of the local amount of steam volume fraction and the radial position of its maximum value. Only at the centre of the pipe the steam volume fraction is still under predicted. The last test of this first investigation consisted of using the improved setup (shift of source points location, consideration of the wall lubrication force, increase of the turbulent dispersion coefficient and use of the Tomiyama heat transfer correlation) and the original injection nozzle diameter in order to evaluate the importance of the radial momentum of steam injection, which was not considered when a larger nozzle diameter was applied in the CFD simulations. The computational time required due to the larger injection velocity was significantly increased. The effect of this modification can be observed in Figure 5 (red solid profile) since the predicted steam volume fraction maximum is thereby moved towards the centre of the pipe.

Detailed results for three of the presented simulations will be shown next. They will be named Configuration 1 (basic setup results - green curve), Configuration 2 (improved

setup - blue curve) and Configuration 3 (improved setup and original nozzle diameter – red curve). Main characteristics in setup of these simulations are summarized in Table 2.

	Config. 1	Config. 2	Config. 3
SP	97[mm]	97[mm]	75[mm]
F _{WL}	-	✓	✓
C _{TD}	1.0	1.5	1.5
Nu	$2 + 0.6 Re_p^{0.5} Pr^{0.3}$	$2 + 0.15 Re_p^{0.8} Pr^{0.5}$	$2 + 0.15 Re_p^{0.8} Pr^{0.5}$
D _{inj}	1[mm]	1[mm]	4[mm]

Table 2: Main CFD setup differences between selected configurations: Location of the source points; consideration of the wall lubrication force; turbulent dispersion coefficient; heat transfer correlation for Nusselt number; injection nozzle diameter.

The cross-sectional averaged steam volume fraction at different steam injection elevations and for the three selected CFD setup configurations are plotted in Figure 6. The horizontal axis corresponds to the distance between steam injection and the measurement plane, being zero at the injection location, and 8m for the largest distance in the TOPFLOW experiment. The results corresponding to the first configuration are able to reproduce the accumulation of steam right after the injection and the trends of the experimental results. However, after L>0.5m the steam volume fraction is strongly over predicted. The second and third configuration behave in a similar way during the first two meters of the pipe after the steam injection. Finally, the prediction using the third CFD configuration shows a good quantitative agreement to the experimental values as well.

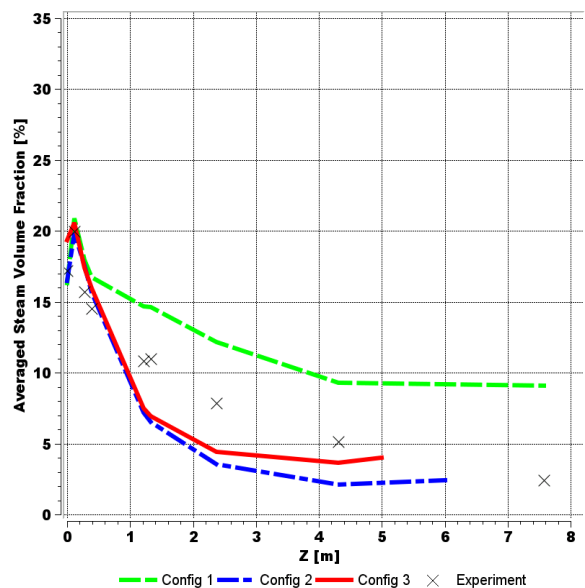


Figure 6: Cross-sectional averaged steam volume fraction at different elevations with respect to the injection level and compared for the three selected CFD configurations.

Figure 7 shows the total steam volume fraction at steady state at a vertical plane between two adjacent injection nozzles for the three different CFD configurations. As already observed in Figure 5 for level *C*, it can be seen that for the first configuration the steam remains all along the pipe near to the wall. This is in contradiction with what was observed during the experiments, where the steam was forming a kind of ring shaped pattern in the measurements. This radial steam distribution is however present at the pictures corresponding to the second and third configuration. Both results are qualitatively analogous. Nevertheless the influence of the nozzle diameter is evident from this comparison, since the steam is slightly shifted towards the centre of the pipe in the third case and a higher amount of steam volume fraction (less recondensation) is predicted along the pipe as well. Detailed results corresponding to the three selected configurations are presented in Figure 8 and Figure 9. Figure 8 shows the radial steam volume fraction distribution at the elevations *A*, *C*, *F*, *I*, *L* and *O* (i.e. measurement at 22, 33, 60, 155, 259 and 451cm above the steam injection location). At elevations *A*, *C* and *F* it can be seen that the first configuration is predicting the steam to remain close to the wall while the distribution of the

steam for the second and third configuration approaches reasonably the experimental results. The larger radial momentum of steam injection in the third CFD configuration causes the steam to move in the direction of the centre of the pipe in comparison with the second configuration. For the upper elevations (*I*, *L* and *O*) less steam is predicted. The second and third configuration results show significant better agreement to the experiments in comparison with the first simulation, and as already observed in Figure 6 the third configuration predicts slightly more steam as the second one. For the same distances between steam injection and measurement cross section the radial bubble size distributions can be analyzed. For all elevations the first configuration is only able to reproduce the location of the maximum of the dr_g/dD_B profile, but due to the strong over prediction of the steam volume fraction in the domain this profile is strongly over predicted as well. The second and third configuration are in much better concordance with the experiments and are able to reproduce reasonably good the experimental values for all investigated steam injection elevations.

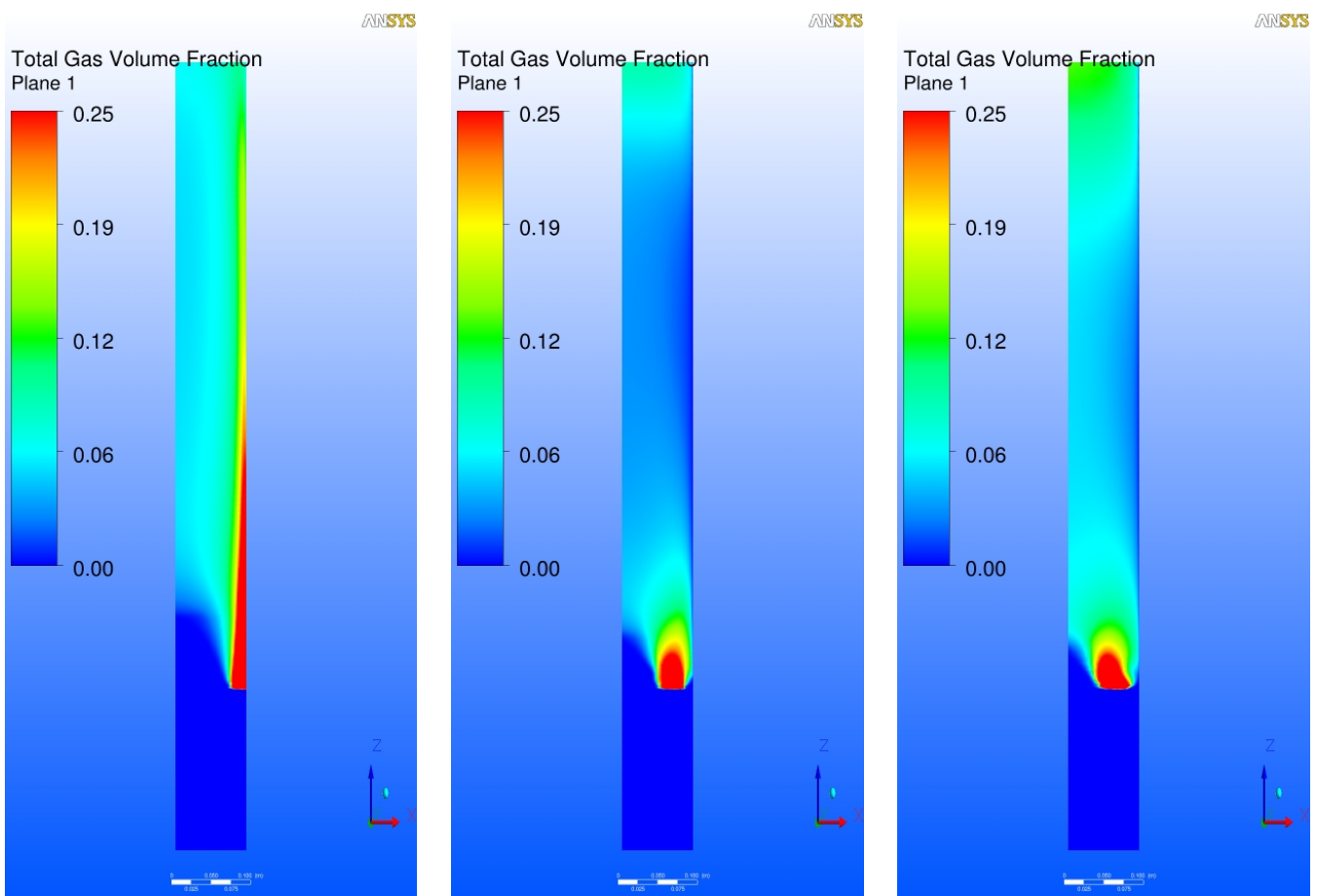


Figure 7: Steady state steam volume fraction at a vertical plane between two adjacent injection nozzles. Left: Configuration 1; Middle: Configuration 2; Right: Configuration 3.

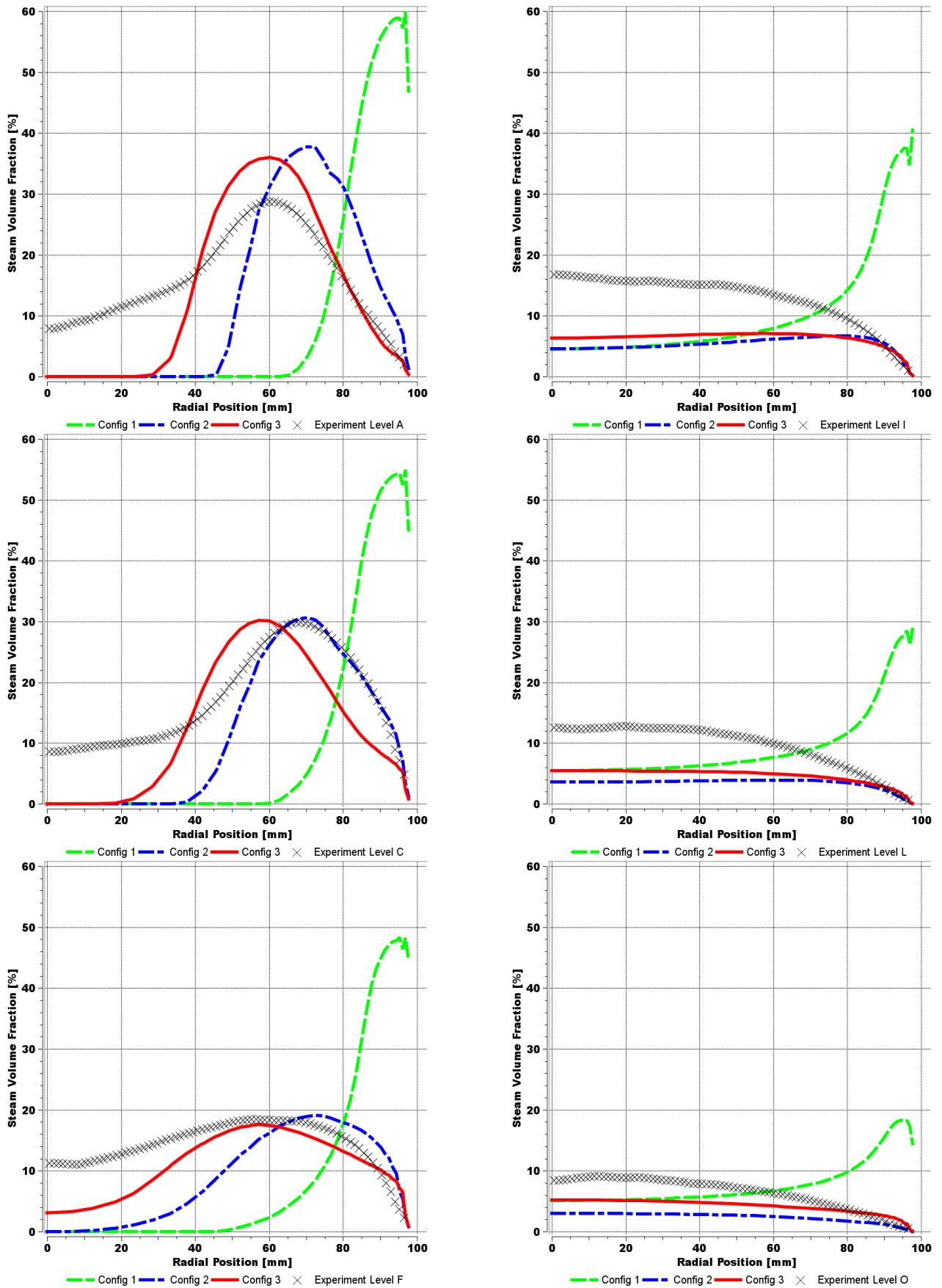


Figure 8: Predicted and experimental radial steam volume fraction distributions at elevations *A*, *C*, *F*, *I*, *L* and *O* (22 cm, 33 cm, 60 cm, 155, 259 and 451 cm respectively above the injection level).

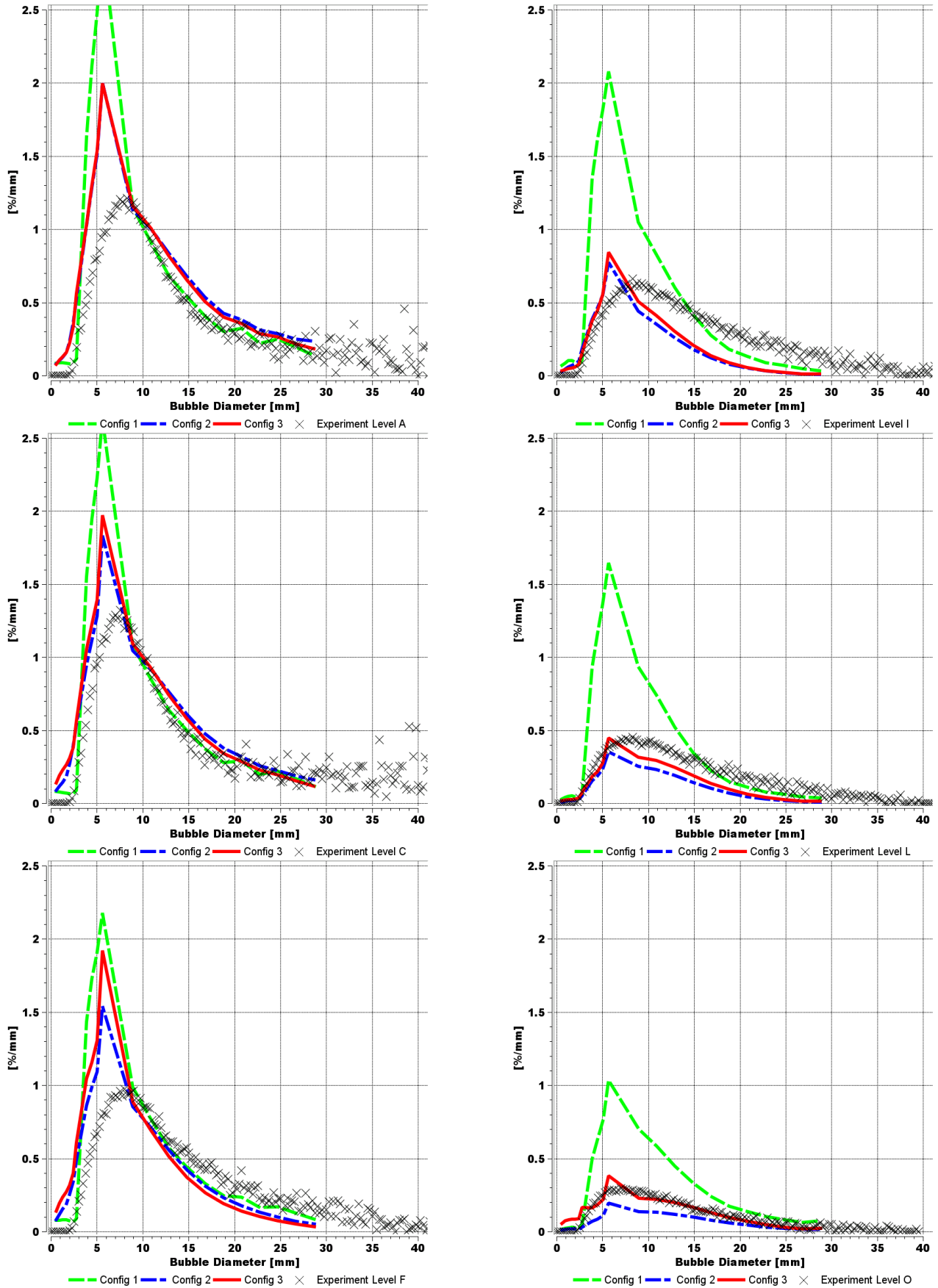


Figure 9: Predicted and experimental radial bubble size distributions (dr_g/dD_B) at elevations *A*, *C*, *F*, *I*, *L* and *O* (22 cm, 33 cm, 60 cm, 155, 259 and 451 cm respectively above the injection level)..

Conclusions

A new methodology to extend the capabilities of the Multiple-size group model (MUSIG) has been presented in this paper. The implemented MUSIG model extension allows simulating two-phase flow applications where not only coalescence and break up of bubbles take place, but where bubble size distribution changes under the influence of mass transfer due to phase change. The new model is able to predict the shrink or growth of bubbles when evaporation or condensation takes place.

The new extended inhomogeneous MUSIG model was developed in collaboration of ANSYS with FZD and has been implemented into a customized solver based on ANSYS CFX 12. In order to validate the extended population balance model for polydisperse bubbly flows a complex water/steam experiment has been chosen. It consists of sub cooled water flowing upwards through the DN200 vertical pipe of TOPFLOW (FZD), into which large amount of steam has been injected. The validation case shows locally values up to 30% of steam volume fraction, where condensation and steam bubble coalescence are the main phenomena taking place. Thanks to the detailed measurements performed at FZD the evolution of the flow along the whole pipe is known, and corresponding measurement data have been used to carry out an extensive analysis of the numerical results obtained by applying the proposed new MUSIG model formulation. Several configurations of the numerical setup have been investigated.. For three of them a detailed comparison against experimental data has been presented. First obtained CFD results (configuration 1) have been improved by modifying some of the numerical parameters and physical submodels. For the so-called configurations 2 and 3, a satisfactory agreement to the experimental data has been obtained. Both simulations are able to reasonably predict the radial steam volume fraction at all elevations along the pipe. The bubble size distribution at the same positions, in terms of the variable dr_g/dD_B has been also investigated, being likewise satisfactorily estimated in the numerical simulations. Results corresponding to the third configuration approach slightly more accurately the experimental investigations than the second one. However, it is also more computational time demanding due to the high steam injection velocities..

Acknowledgements

This research has been supported by the German Ministry of Economy (BMW) under the contract number 150 1328 in the framework of the German CFD Network on Nuclear Reactor Safety Research and Alliance for Competence in Nuclear Technology, Germany.

References

ANSYS Inc. 2009. *ANSYS CFX 12 Users Manual*. 2009.

Frank, T. 2006. *Entwicklung von CFD-Software zur Simulation mehrdimensionaler Strömungen im Reaktorkühlsystem*. Otterfing : s.n., 2006. ANSYS TR-06-01.

Frank, T, et al. 2006. *Validation of CFD models for mono and polydisperse air-water two-phase flows in pipes*. Garching : s.n., 2006, CFD4NRS Workshop on Benchmarking of CFD Codes for Application to Nuclear Reactor Safety.

Krepper, E. 2008. *The inhomogeneous MUSIG model for the simulation of polydispersed flows*. 2008, Nuclear Engineering and Design, Vol. 238, p. polydispersed flows.

Krepper, E, Lucas, D and Prasser, H-M. 2005. *On the modelling of bubbly flow in vertical pipes*. 2005, Nuclear Engineering and Design, Vol. 235, pp. 597-611.

Lifante, C, et al. 2009a. *Entwicklung von CFD-Software zur Simulation mehrdimensionaler Strömungen in Reaktor-kühlsystemen*. Otterfing : s.n., 2009. ANSYS/TR-09-02.

Lifante, C, et al. 2009b. *Extension of the Multiple-Size Group (MUSIG) Model to Phase Change Effects*. Dresden : s.n., 2009, Workshop on Multiphase Flows, Simulation, Experiment and Application.

Lucas, D and Prasser, H-M. 2007. *Steam bubble condensation in sub-cooled water in case of co-current vertical pipe flow*. Steam bubble condensation in sub-cooled water in case of co-current vertical pipe flow. *Nuclear Engineering and Design*. 2007, Vol. 237, 5, pp. 497-508.

Lucas, D, et al. 2008. *Benchmark database on the evolution of two-phase flows in a vertical pipe*. Grenoble : s.n., 2008, XCFD4NRD, Experiments and CFD Code Applications to Nuclear Reactor Safety.

Lucas, D, Krepper, E and Prasser, H-M. 2001. *Prediction of radial gas profiles in vertical pipe flow on basis of the bubble size distribution*. 2001, International Journal of Thermal Sciences, Vol. 40, pp. 217-225.

Lucas, D, Krepper, E and Prasser, H-M. 2007. *Use of models for lift, wall and turbulent dispersion forces acting on bubbles for poly-disperse flows*. 2007, Chemical Science and Engineering, Vol. 62, pp. 4146-4157.

Luo, S.M. and Svedensen, H. 1996. *Theoretical Model for Drop and Bubble Breakup in Turbulent Dispersions*. 1996, AIChE Journal, Vol. 42, pp. 1225 -1233.

Menter, F. 1994. *Two-equation eddy-viscosity turbulence models for engineering*. 1994, AIAA-Journal, Vol. 8.

Prasser, H-M, et al. 2007. *Evolution of the structure of a gas-liquid two-phase flow in a large vertical pipe*. 2007, Nuclear Engineering and Design, Vol. 237, pp. 1848-1861.

Prince, M and Blanch, H. 1990. *Bubble Coalescence and Break-Up in Air-Sparged Bubble Columns*. 1990, AIChE Journal, Vol. 36.

Tomiya, A. 2009. *Progress in Computational Bubble Dynamics*. Dresden : s.n., 2009, Workshop on Multiphase

Flows. Simulation, Experiment and Application.

Tomiyama, A. 1998. *Struggle with computational bubble dynamics*. Lyon : s.n., 1998, 3rd International Conference on Multiphase Flow.